Sawtooth-wave adiabatic-passage slowing of dysprosium

N. Petersen,[1,2] F. Mühlbauer,[1] L. Bougas,[3] A. Sharma,[3] D. Budker,[1,3,4] and P. Windpassinger[1,2]
[1]*QUANTUM, Institut für Physik, Johannes Gutenberg-Universität, 55099 Mainz, Germany*
[2]*Graduate School Materials Science in Mainz, Staudingerweg 9, 55128 Mainz, Germany*
[3]*Helmholtz Institut Mainz, Johannes Gutenberg-Universität, Staudingerweg 18, 55128 Mainz, Germany*
[4]*Department of Physics, University of California, Berkeley, California 94720-7300, USA*

(Received 29 April 2019; published 17 June 2019)

We report on sawtooth-wave adiabatic-passage (SWAP) slowing of bosonic and fermionic dysprosium isotopes by using a 136-kHz-wide transition at 626 nm. A beam of precooled atoms is further decelerated in one dimension by the SWAP force and the amount of atoms at near zero velocity is measured. We demonstrate that the SWAP slowing can be twice as fast as in a conventional optical molasses operated on the same transition. In addition, we investigate the parameter range for which the SWAP force is efficiently usable in our setup and relate the results to the adiabaticity condition. Furthermore, we add losses to the hyperfine ground-state population of fermionic dysprosium during deceleration and observe more robust slowing with SWAP compared to slowing with the radiation pressure force.

DOI: 10.1103/PhysRevA.99.063414

Laser cooling is an important prerequisite in many research areas like quantum gases [1–3], ion traps [4], and optical atomic clocks [5]. A commonly applied method to cool atoms is radiation pressure (RAD) cooling, which is based on directed absorption of photons by the atoms and subsequent spontaneous emission. That way, temperatures in the mK to μK range are typically reached. The minimal temperature and the maximum force and velocity-capture range are limited by the decay rate Γ from the upper state of the used transition [1]. Relying on spontaneous emission for cooling requires the transition to be closed or at least nearly closed such that repumping from "dark states" is feasible.

Extending laser cooling to multifrequency light fields can overcome some of the limitations of RAD cooling [6], particularly the maximum achievable force and the velocity-capture range. Examples are the bichromatic force [7–11] and forces originating from pulsed rapid adiabatic passages [12–14].

Recently, a cooling technique called sawtooth-wave adiabatic passage (SWAP) was demonstrated for strontium [15–17] on a $2\pi \times 7.5$ kHz wide transition and rubidium on a Raman transition [18]. In this work, we demonstrate its application for dysprosium (Dy). We use the $\Gamma_{626} = 2\pi \times 136$ kHz transition from the ground-state at 626 nm [Fig. 1(a)] with a saturation intensity of $I_S = 72\ \mu\mathrm{W/cm^2}$ [19–21] to generate the SWAP force. Thereby, we validate that the SWAP force also works for more than one order of magnitude broader transitions than previously demonstrated. The 626-nm transition is comparable in terms of linewidth and saturation intensity to the $2\pi \times 160$ kHz $X\,^2\Sigma \rightarrow A'\,^2\Delta_{3/2}$ transition in YO [22]. To show the robustness of the process, we exploit the hyperfine structure of fermionic ^{163}Dy [Fig. 1(b)] and use it to induce ground-state losses during the deceleration.

Similar to the bichromatic force and pulsed rapid adiabatic passage, the SWAP force does not rely on spontaneous photon scattering to remove kinetic energy, but uses rapid adiabatic passages for the excitation as well as for the emission processes and is experimentally straightforward to implement. It is expected to have several advantages over the RAD force

$$F_{\mathrm{RAD,max}} = \frac{\hbar k}{2}\Gamma, \tag{1}$$

which is given here for a saturated transition and a resonant laser beam [1]. First, the maximum SWAP force is not limited by the decay rate from the upper state and, thus, in principle, even with narrow transitions strong forces can be generated when high ramp repetition rates are applied and the adiabaticity condition is fulfilled. Furthermore, SWAP cooling is expected to remove considerably more atomic momentum per spontaneously scattered photon compared to RAD cooling and hence the requirement to find a closed cooling transition can be relaxed [25]. This is of special interest for cooling of molecules and in general of systems with open transitions. Due to fewer spontaneous decays being involved, the SWAP force may be also advantageous for cooling optically dense samples, where spontaneously emitted photons could be radiationally trapped and may reduce the cooling efficiency otherwise.

To briefly recapitulate the basic principle, let us consider an atom moving with velocity v in one dimension in the presence of two near-resonant, counterpropagating laser beams. The frequency ω of these laser beams, which is the same for both beams, is swept symmetrically around the atomic transition frequency ω_{res} in a sawtooth pattern as shown in Fig. 1(c). For an atom moving with velocity v, the frequencies of the beams will appear Doppler shifted in opposite directions. This induces time ordering in the absorption of the photons from the two counterpropagating beams. For increasing frequency ramps, the beam counterpropagating to the moving atom will first induce an adiabatic transfer of the atom from the ground state to the upper state. After a specific amount of time, which is determined by the velocity of the atom and the slope of the frequency ramp, the copropagating beam induces

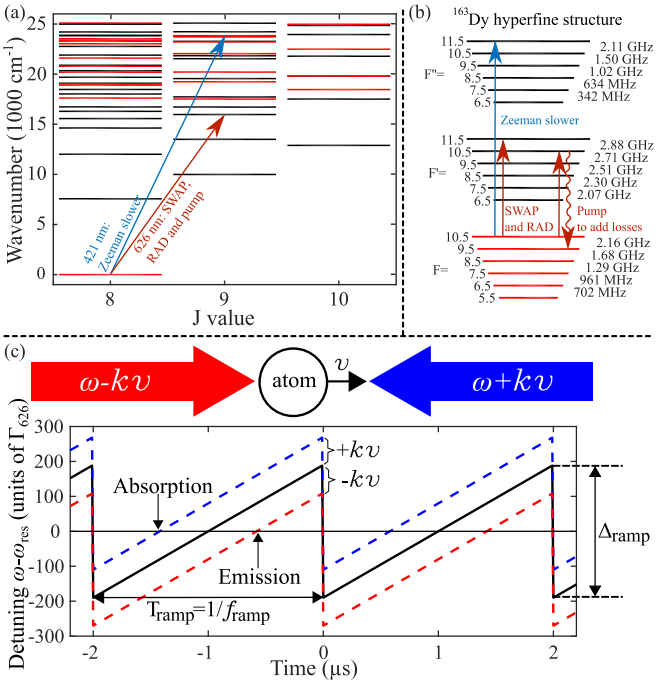

FIG. 1. (a) Excerpt of Dy energy levels for total angular momenta $J = 8$, 9, and 10 [23]. Even (odd) parity levels are drawn in red (black). (b) Hyperfine structure of the ^{163}Dy isotope [20,24]. The arrows indicate the transitions used for the Zeeman slower at 421 nm, for the SWAP deceleration at 626 nm, and for the implementation of ground-state losses. (c) Schematic of the SWAP force mechanism. The black sawtooth function describes the time-dependent detuning of the counterpropagating laser beams with respect to an atom at rest. An atom moving with finite velocity v experiences Doppler-shifted frequency ramps indicated by the blue and red dashed lines in the plot. Important parameters of the sawtooth ramps used for deceleration of dysprosium like the ramp amplitude Δ_{ramp} and ramp repetition rate f_{ramp} are indicated.

rapid adiabatic passage from the excited state back to the ground state. During both events, one photon momentum is transferred to the atom in the direction opposite to its motion. The jump in frequency back to red detuning must be diabatic such that the atom stays in the ground state. In this way, an average force of

$$F_{\text{SWAP}} = 2\hbar k f_{\text{ramp}} \tag{2}$$

is acting on the atom, where k is the wave number of the used transition and f_{ramp} is the repetition rate of the frequency ramp. If one inverts the slope of the sawtooth ramp, the time ordering of the adiabatic passages is inverted and the atom gets accelerated. To be in the adiabatic regime, the condition

$$\kappa = \frac{\Omega_0^2}{\alpha} = \frac{\Omega_0^2}{f_{\text{ramp}}\Delta_{\text{ramp}}} \gg 1 \tag{3}$$

needs to be fulfilled [25]. Here, κ is the adiabaticity parameter, α is the slope of the ramp, Δ_{ramp} is the ramp amplitude, and Ω_0 is the on-resonance Rabi frequency. This description of the SWAP force is only valid as long as the resonance crossing times of the counter- and copropagating beams are well separated in time, which depends on the Rabi frequency of the laser beams and the velocity of the atom. The authors of Ref. [25] investigated SWAP cooling in the adiabatic regime and found that the resonances keep separated if

$$|\Omega_0| < \left| kv - \frac{\hbar k^2}{m} \right|, \tag{4}$$

with m being the mass of the atom and v its velocity. They refer to this condition as the high-velocity regime and point out that atoms outside of this regime may still be cooled but the dynamics are more difficult to describe and analyze qualitatively.

I. EXPERIMENTAL SCHEME

The experimental setup is depicted in Fig. 2(a). A continuous beam of decelerated Dy atoms leaves a Zeeman slower (ZS) described in Ref. [26]. The atoms have a typical velocity distribution featuring a peak at about 20 m/s and a tail extending to even negative velocities as shown in Figs. 6(b) and 6(d) in Appendix A. Two circularly polarized laser beams counterpropagate collinearly with a homogeneous 1.7-G magnetic field directed at 45° relative to the ZS axis. They are turned on, typically, for 1 ms. The beams are either red detuned from the 626-nm transition of Dy to act as an optical molasses

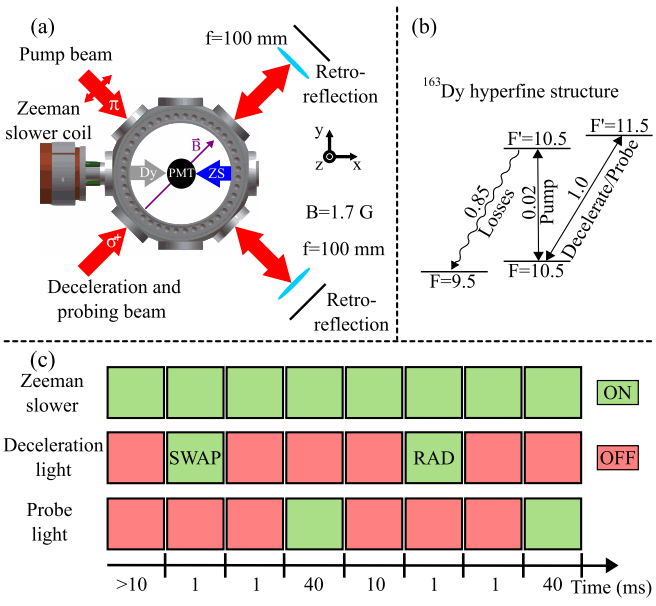

FIG. 2. (a) Schematic of the vacuum chamber inside which the SWAP or RAD deceleration takes place. The gray arrow labeled "Dy" indicates the direction of atoms leaving the ZS after deceleration by the ZS beam labeled "ZS". The direction of the magnetic field used as quantization axis is drawn in purple and the retro-reflected pump and probe beams are indicated by red arrows along with their polarizations. The photomultiplier tube used for the fluorescence measurements is placed below the vacuum chamber and is labeled "PMT". (b) The part of the ^{163}Dy hyperfine structure that is relevant for the described experimental scheme. The numbers next to the transition arrows indicate the relative transition strengths normalized to the $F = 10.5 \rightarrow F' = 11.5$ transition. (c) Sequence used to compare the RAD and SWAP force. When losses are added to the $F = 10.5$ ground-state, the pump beam is switched on during the deceleration.

or modulated in the sawtooth manner shown in Fig. 1(c) to decelerate the atoms. Their $1/e^2$ beam diameter is 1.7 cm and the beams pass a 1.4-cm-diameter aperture before entering the vacuum chamber. After deceleration, the laser beams are switched off for 1 ms as shown in Fig. 2(c). They are then switched on again with a typical intensity corresponding to a saturation parameter $S = I/I_S = 24$ and on resonance to the 0 m/s velocity class for probing the amount of slow atoms. The 0 m/s velocity class atoms exhibit a Doppler-free fluorescence peak in this experimental geometry. This fluorescence is measured with a photomultiplier tube for 40 ms and the initial intensity, which decays due to atoms moving out of the probe beam in typically 6 ms, is taken as a measure of the amount of atoms at 0 m/s. For further analysis, the background signal, which stems partially from atoms that have been slowed to 0 m/s by the ZS prior to the RAD or SWAP deceleration, is subtracted. In the data presented in Sec. II, this background-subtracted fluorescence intensity of the 0 m/s velocity class is plotted either as absolute values I_{SWAP} or I_{RAD} after SWAP or RAD deceleration, respectively, or as the ratio I_{SWAP}/I_{RAD}. To compare the SWAP and RAD forces directly, the deceleration and probing sequence is repeated alternatingly for RAD and SWAP. In the case of ^{163}Dy the ZS pumps the atoms to the $F = 10.5$ hyperfine ground state.

Losses can be added to the ground state by applying a pump beam on the $F = 10.5 \rightarrow F' = 10.5$ transition during the deceleration as shown in Fig. 2(b). More details on the Doppler-free fluorescence signals and the SWAP setup can be found in Appendices A and B.

II. EXPERIMENTAL RESULTS

Unless otherwise noted, all measurements presented here are conducted using ^{163}Dy but similar results were also achieved with ^{162}Dy. In Fig. 3 we compare the fluorescence intensities I_{SWAP} and I_{RAD} for different ramp repetition rates f_{ramp}. Both forces are generated with beams having the same peak-saturation parameter S = 2600. In the case of the RAD, an optimized red detuning of $\Delta_{RAD} = -15.5\,\Gamma_{626}$ is applied. For SWAP, we use a ramp amplitude of $\Delta_{ramp} = 190\,\Gamma_{626}$ with a zero mean detuning. Initially, the amount of slow atoms increases with f_{ramp} as expected from Eq. (2). At $f_{ramp} = 200$ kHz, the SWAP force surpasses the RAD force, and at $f_{ramp} = 500$ kHz, it is twice as large. Further increase of f_{ramp} does not lead to significantly higher numbers of 0 m/s atoms, and beyond $f_{ramp} = 1.5$ MHz, the amount of slow atoms decreases. This can be related to the decrease of the adiabaticity parameter, which is $\kappa = 3.9$ at 1.5 MHz compared to $\kappa = 11.7$ at 500 kHz. When we invert the slope of the sawtooth ramps, the amount of atoms in the 0 m/s velocity class decreases to negative values, which means that the atoms are now accelerated as discussed above. For $f_{ramp} \geqslant$ 1.5 MHz fewer atoms are accelerated in accordance with the less efficient deceleration for rising ramps in this regime.

To further explore the relative efficiency of SWAP deceleration versus RAD deceleration, we compare the two techniques for different deceleration times at $f_{ramp} = 500$ kHz. The results are shown in Fig. 4. Both forces lead to a linear increase of slow atoms over the first 0.75 ms until saturation sets in above about 1 ms. The saturation could be

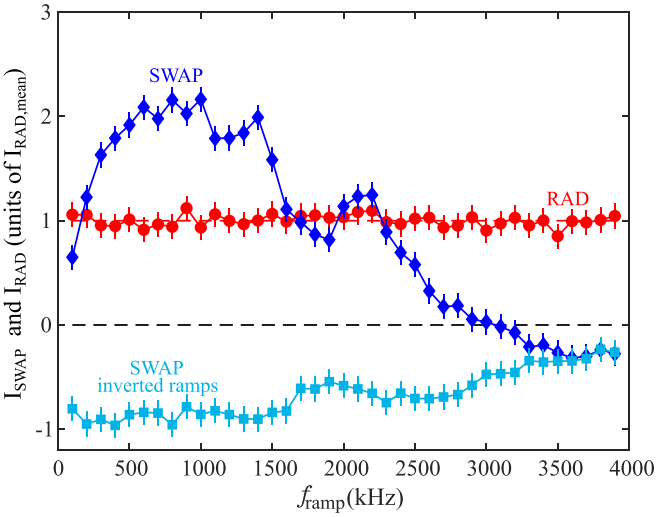

FIG. 3. SWAP deceleration is applied for 1 ms for varying ramp repetition rates f_{ramp} (dark blue diamonds) and subsequently I_{SWAP} is measured. For comparison, RAD deceleration is applied for the same amount of time and the same saturation parameter with an optimized red detuning $\Delta_{RAD} = -15.5\ \Gamma_{626}$ (red circles). The measured intensities are normalized to the mean intensity after RAD deceleration $I_{RAD,mean}$. When the slope of the sawtooth ramp is inverted, we measure negative background-subtracted fluorescence intensities (light blue squares). To estimate the error of the measured intensities we perform 270 measurements at $f_{ramp} = 400$ kHz and determine the standard deviation σ of I_{SWAP} and I_{RAD}. The error bars in this figure are the standard error $\sigma/\sqrt{N}$, with $N = 15$ being the number of measurements done for each f_{ramp} setting.

due to an equilibrium reached between new atoms entering the deceleration beam region and atoms leaving the beam region due to remaining velocity components perpendicular to the deceleration beams and due to gravity. An increase of slow atoms for deceleration times longer than 6 ms is not expected since the fluorescence signals decay to the background level on a comparable time scale. The saturated I_{SWAP} is about 24% larger than the saturated I_{RAD} which indicates that the SWAP force decelerates atoms from the ZS beam more efficiently. From the slope of the linear range we conclude that the SWAP force decelerates a factor of 2.1 more atoms per time than the RAD force does. The SWAP force at 500 kHz is expected to be 2.3 times stronger than the RAD force for the saturated 626-nm transition [Eq. (1)]. A larger velocity-capture range would also explain a higher slope, but the capture ranges of the two forces for our set of parameters are theoretically almost equal. In the case of the RAD force the power-broadened capture range is $v_{c,RAD} = \Gamma_{626}\sqrt{S+1}/k_{626} = 4.3$ m/s [1,6] while in the case of the SWAP force it is $v_{c,SWAP} = \Delta_{ramp}/(4k_{626}) = 4.0$ m/s, with k_{626} being the angular wave number of the 626-nm transition [25]. To check this, we compare SWAP results in Fig. 4(b) for different ramp repetition rates but equal ramp amplitude Δ_{ramp} and hence equal capture range. The increase of I_{SWAP} for rising ramp repetition rates indicates that the 2.1 faster accumulation of atoms in the 0 m/s velocity class is mainly due to a larger force and not due to a larger capture range of the SWAP force.

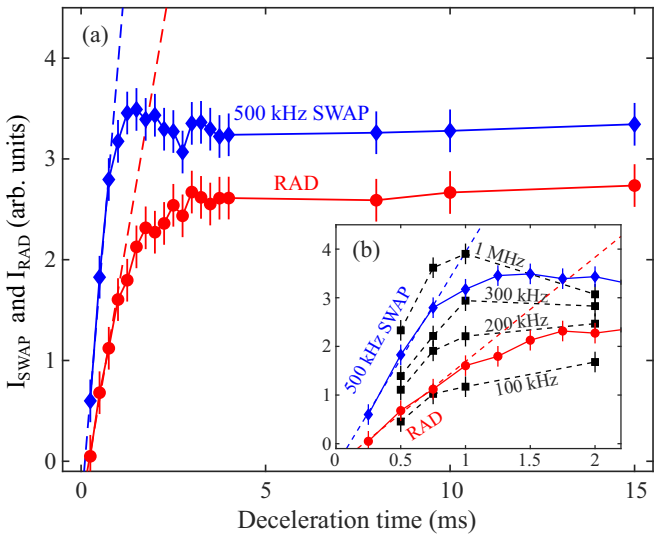

FIG. 4. (a) I_{SWAP} (dark blue diamonds) and I_{RAD} (red circles) are compared for increasing deceleration time. The SWAP and RAD beam settings and the error calculations are the same as for the data in Fig. 3. The dashed lines are the result of a linear fit to the first three data points. (b) A zoom into the data points of panel (a) up to 2 ms. In addition, results for SWAP deceleration with different ramp repetition rates but equal velocity-capture ranges are shown as black squares.

In addition to the measurements presented here, we perform an independent optimization of the RAD force for both ^{162}Dy and ^{163}Dy including spectral broadening of the deceleration-beams. With the same deceleration-beam intensity for both forces and a deceleration time of 0.75 ms, no spectral broadening and detuning parameters are found for which the ratio I_{RAD}/I_{SWAP} becomes larger than 0.55 with $f_{ramp} = 500$ kHz and $\Delta_{ramp} = 190\ \Gamma_{626}$.

In Fig. 5 we plot the ratio I_{SWAP}/I_{RAD} for different combinations of parameters (Ω_0, f_{ramp}, and Δ_{ramp}) as a measure of the efficiency of SWAP deceleration over RAD deceleration. For these measurements, the RAD beams are set to a fixed red detuning of $\Delta_{RAD} = -15.5\ \Gamma_{626}$ and their intensity is equal to the intensity of the SWAP beams. For the data in Fig. 5(a) we vary the Rabi frequency Ω_0 of the SWAP and RAD beams while $\Delta_{ramp} = 190\ \Gamma_{626}$ is fixed, and for Fig. 5(b) we vary the ramp amplitude Δ_{ramp} while $\Omega_0^2 = 860 \times 10^{12}\ s^{-2}$ ($S = 2350$) is fixed. For reference, lines at which κ is constant are plotted also. The data shown in Fig. 5(a) demonstrate that the SWAP force maintains a factor of 2 higher deceleration rates than the RAD force over a large range of Rabi frequencies. Additionally, one observes that the mean position of the maximum I_{SWAP}/I_{RAD} shifts to higher ramp repetition rates when higher Ω_0^2 values are applied as expected from the adiabaticity condition, but it does not strictly follow one of the $\kappa = $ const. lines. For increasing Ω_0^2, the maximum is located at higher κ values, indicating that not only the adiabaticity condition is limiting the highest usable ramp repetition rates. As pointed out at the end of the Introduction the simple description of the SWAP force, where two photon momenta per frequency ramp are transferred to the atom in the opposite direction of its motion, is only valid in the high-velocity regime. For increasing Rabi frequencies the lower velocity limit of the high-velocity regime also increases according to Eq. (4). Since the SWAP capture range should be on the order of 4.0 m/s most of the atoms in the higher Ω_0^2 data sets were probably already below the high-velocity regime before the deceleration started, which could have reduced the efficiency of SWAP slowing. The data shown in Fig. 5(b) indicates that even larger I_{SWAP}/I_{RAD} ratios could be reached for larger Δ_{ramp} values but these are limited in our setup to about 190 Γ_{626} for technical reasons. When Δ_{ramp} is increased the I_{SWAP} maximum moves to lower f_{ramp} values as expected from the adiabaticity condition. The increase of I_{SWAP} with larger ramp amplitudes is probably caused by the increase of the capture range of the SWAP force, which is only 2 m/s at 95 Γ_{626} compared to 4 m/s at 190 Γ_{626}. Interestingly, while Δ_{ramp} is increased the absolute I_{SWAP} maximum moves to lower f_{ramp} values but a second local maximum at higher f_{ramp} moves further to higher f_{ramp} values in the opposite direction.

The development of new laser-cooling techniques, which are robust against population loss from the upper state and lower state of the used transition, is of great interest for

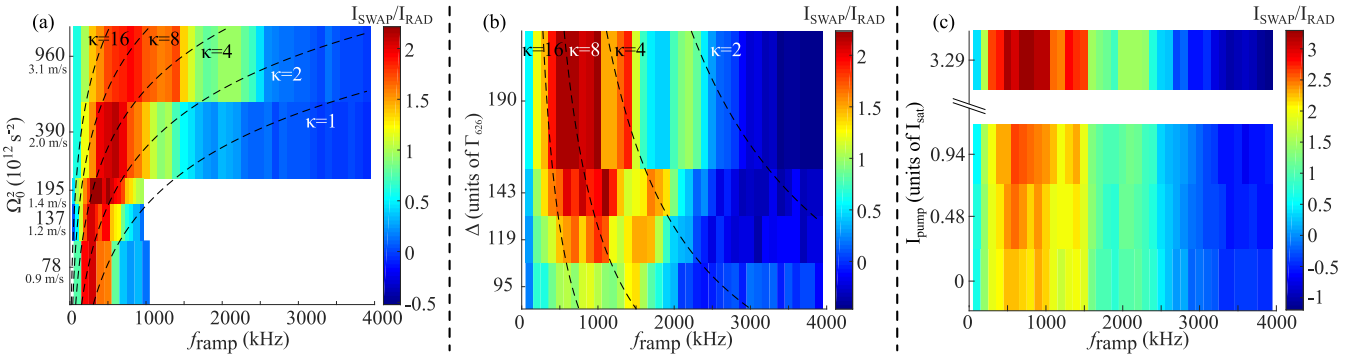

FIG. 5. All three graphs show the ratio I_{SWAP}/I_{RAD} as a measure of the SWAP deceleration efficiency. In panels (a) and (b) the dashed lines indicate lines of a constant adiabaticity parameter κ. (a) For a fixed SWAP ramp amplitude $\Delta_{ramp} = 190\ \Gamma_{626}$ the squared Rabi frequency Ω_0^2 and the ramp repetition rate f_{ramp} are varied. For this data set, ^{162}Dy is used. The velocities below the squared Rabi frequencies denote the lower limits to the high-velocity regime. (b) For a fixed $\Omega_0^2 = 860 \times 10^{12}\ s^{-2}$ the ramp amplitude Δ_{ramp} and the ramp repetition rate f_{ramp} are varied. (c) The intensity of the pump beam, I_{pump}, which induces losses to the $F = 10.5$ ground state is increased stepwise and plotted versus f_{ramp}. The deceleration time is 1 ms for the data presented in panels (a) and (c) and 0.75 ms for the data plotted in panel (b).

experiments with atoms or molecules, which have complex electronic structures with many possible decay channels. To simulate the robustness against an unstable ground state, we actively pump population out of the ground state into a level not used for cooling. To this end, we add losses to the $F = 10.5$ ground state of ^{163}Dy during SWAP and RAD deceleration by applying a pump beam that is resonant with the $F = 10.5 \rightarrow F' = 10.5$ transition as shown in Fig. 2(b). The amount of losses is increased stepwise by increasing the pump-beam intensity I_{pump} and the results are shown in Fig. 5(c). The corresponding Rabi frequencies range from $2\pi \times 10$ kHz ($0.48\, I_{\text{sat}}$) to $2\pi \times 27$ kHz ($3.29\, I_{\text{sat}}$). While after both, SWAP and RAD deceleration, losses of slow ground-state atoms are observed, the ratio $I_{\text{SWAP}}/I_{\text{RAD}}$ increases by 50 % for $I_{\text{pump}} = 3.29\ I_{\text{sat}}$ at $f_{\text{ramp}} = 700$ kHz compared to $I_{\text{pump}} = 0$. Thus the SWAP force is less influenced than the RAD force by the added loss mechanism. We also study the dependence of the ground-state losses on the detuning of the pump beam to the $F = 10.5 \rightarrow F' = 10.5$ transition and present the results in Appendix C. In order to rule out possible coherent two-photon processes from the pump and cooling beams, we add phase noise to the pump laser beam with a 3-dB bandwidth of 6 MHz and phase noise amplitudes ranging from 0 to 2π. Neither I_{SWAP} nor I_{RAD} is influenced by adding phase noise at $I_{\text{pump}} = 3.29\ I_{\text{sat}}$ and $f_{\text{ramp}} = 500$ kHz.

III. CONCLUSIONS

We have demonstrated one-dimensional deceleration of Dy by the recently developed SWAP technique. For identical beam intensities and similar velocity-capture ranges, we observe that the SWAP force is by a factor of 2.1 times faster in decelerating atoms than the RAD force. Our study of the SWAP parameter range should facilitate the integration of SWAP forces into experiments with various other atomic species as well as molecules. Furthermore, we observe a higher robustness of the SWAP force against ground-state losses, which were induced by opening a decay channel to another hyperfine ground state. It will be a subject of future studies to implement a loss channel for the upper state of the deceleration transition.

ACKNOWLEDGMENTS

The authors thank Carina Baumgärtner and Lena Maske for their contributions to the experiment. We gratefully acknowledge financial support by the JGU-Startup funding, the DFG-Grossgerät INST 247/818-1 FUGG, and the Graduate School of Excellence MAINZ (GSC 266).

APPENDIX A: VELOCITY-SELECTIVE SATURATED FLUORESCENCE SPECTROSCOPY

To determine the number of atoms in the 0 m/s velocity class, we use a method similar to velocity-selective saturated fluorescence spectroscopy (VSSFS) as used by Gao *et al.* [27]. As depicted in Fig. 6(a), we use two counterpropagating laser beams at 45° to the atomic beam. When the two laser beams are symmetrically detuned by $\pm\Delta f/2$ around the atomic resonance frequency f_{res} of the 626-nm transition, only atoms

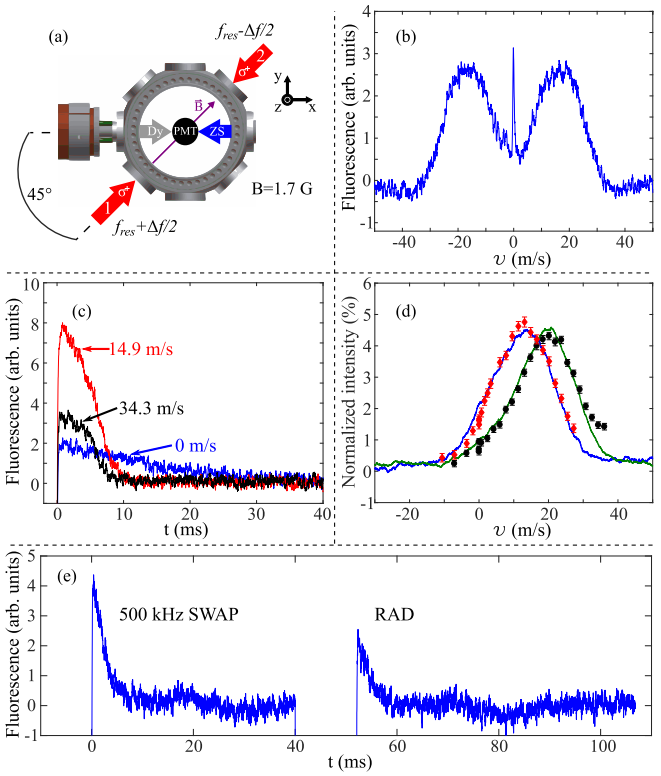

FIG. 6. (a) Sketch of the setup used for measuring the velocity distribution of atoms leaving the ZS. The velocity measurement is done in 45° to the x axis while all velocities given in this figure are transformed to be along the x axis, which is the atomic beam direction. (b) Fluorescence spectrum obtained by scanning two counterpropagating laser beams as shown in panel (a) with $\Delta f = 0$. The Doppler-free fluorescence signal is visible at 0 m/s and its FWHM is about 0.45 m/s. (c) Decaying fluorescence signals of atoms with 0, 14.9, and 34.3 m/s velocity in the x direction plotted in blue, red, and black, respectively, after suddenly switching off the ZS. The initial intensity is measured by averaging the signals over a time span of 0.6 ms after switching on the probe beams at time $t = 0$. (d) For two different current settings of the ZS two continuous velocity spectra in blue and green are measured by using and scanning only beam 2 marked in panel (a). The red and black data points are results for the same ZS settings but are measured by VSSFS. The normalization of these intensities is described in the main text. (e) Typical fluorescence signals measured with the sequence outlined in Fig. 2(c) to obtain I_{SWAP} and I_{RAD}.

with the velocity

$$v = \lambda_{626}\Delta f/[2\cos(45^\circ)] \tag{A1}$$

are resonant with both beams at the same time. Here the atoms are assumed to move on average into the x direction along the ZS axis. When both beams are scanned in frequency while maintaining a fixed relative detuning $\Delta f = 0$, one obtains the velocity spectrum shown in Fig. 6(b), where two broad peaks are visible. The fluorescence of the right (left) peak is caused by laser beam number 1 (laser beam number 2) and the sharp peak in the center is a Doppler-free fluorescence signal with a full width at half maximum (FWHM) of 0.45 m/s caused by both beams.

To perform the atom-number measurements presented in the main text the laser frequency is stabilized to the 0 m/s velocity class at $\Delta f = 0$. By applying probe beams with varying Δf after switching off the ZS, one can measure the decaying fluorescence of different velocity classes. The initial fluorescence after switching off the ZS is proportional to the amount of atoms in the respective velocity class associated with the chosen Δf. In Fig. 6(c) three such fluorescence signals are shown for 0, 14.9, and 34.3 m/s. For increasing velocity, the temporal shape of the fluorescence signals becomes more boxlike. This is expected for a continuous stream of atoms, which have a certain velocity, that is cut off suddenly. The time of the decay to the background level agrees well with the velocities associated with the used detunings and the distance of the last ZS coil to the end of the probe-beam interaction region, which is about 23 cm. To demonstrate that VSSFS is suitable to selectively measure the amount of atoms in certain velocity classes, we compare standard one-beam Doppler spectroscopy to the results when VSSFS is used in Fig. 6(d) and observe a good agreement between the two methods. The VSSFS and the standard Doppler spectra are normalized to the integral over the velocities covered by the VSSFS measurements. Typical fluorescence signals of the 0 m/s velocity class are plotted in Fig. 6(e). I_{SWAP} and I_{RAD} are measured by averaging the intensity over a time span of 0.6 ms after switching on the probe beams.

APPENDIX B: GENERATION AND MEASUREMENT OF SAWTOOTH FREQUENCY RAMPS

In this section we describe how a sawtooth-frequency-modulated laser beam is generated in our setup and how we switch between the SWAP beam, the RAD beam, and the probe beam. To modulate the frequency and control the intensity, the laser beam is focused through an acousto-optic modulator (AOM) with a 52-μm beam waist in a double-pass configuration. After passing through the AOM twice, the beam is coupled into a single-mode fiber and guided to the vacuum main chamber. In Fig. 7(a) a schematic of the radio-frequency (RF) electronics, which drive the AOM, is shown. There are two sources of AOM driving frequencies. A direct digital synthesizer generates a 95-MHz sine wave, which is amplified to drive the AOM during the time when probing is performed. The second RF source consists of a voltage controlled oscillator (VCO), which is controlled by the output of a function generator. The function generator drives the VCO with either sawtooth waves for the SWAP deceleration or with a constant voltage for RAD deceleration. The VCO output frequency at about 207 MHz is mixed down to 95 MHz before it is amplified and sent to the AOM while the last amplifier also acts as a low-pass filter, which cuts off the higher frequencies leaving the mixer. With the RF switch we choose between the probe beam and the SWAP and RAD beam settings. To verify that this setup can modulate the laser beam with sawtooth frequency ramps, we measure the beat between a constant-frequency laser beam and the SWAP beam on a photodiode. The frequency of the beat signal is for technical reasons centered around 400 MHz. By fitting sine functions to 25-ns-long segments of the beat signal, the instantaneous beat frequency is obtained. The results for two settings of the ramp repetition rate are plotted in Fig. 7(b) versus time and show the expected sawtooth form.

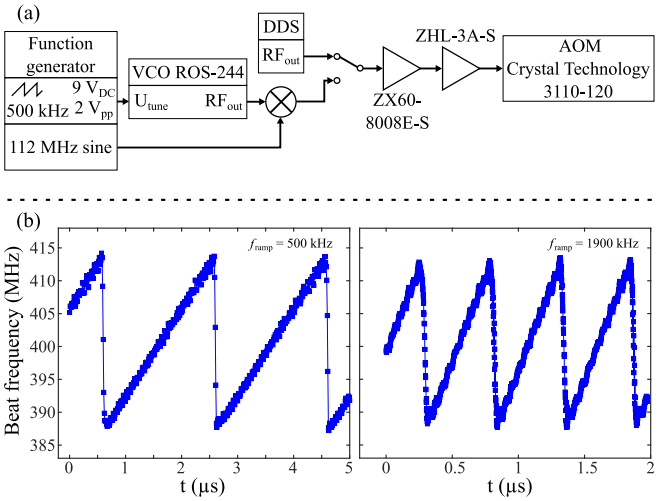

FIG. 7. (a) Schematic of the RF electronics used to generate the sawtooth frequency ramps at around 95 MHz to drive the SWAP double-pass AOM. All components except the function generator, the AOM, and the direct digital synthesizer (DDS) are manufactured by Mini-Circuits. (b) Results of an optical beat measurement between a constant-frequency laser beam and a laser beam that is modulated with $\Delta_{\mathrm{ramp}} = 190\ \Gamma_{626}$ and $f_{\mathrm{ramp}} = 500$ kHz (left) and $f_{\mathrm{ramp}} = 1900$ kHz (right) sawtooth waves by using the setup outlined in panel (a).

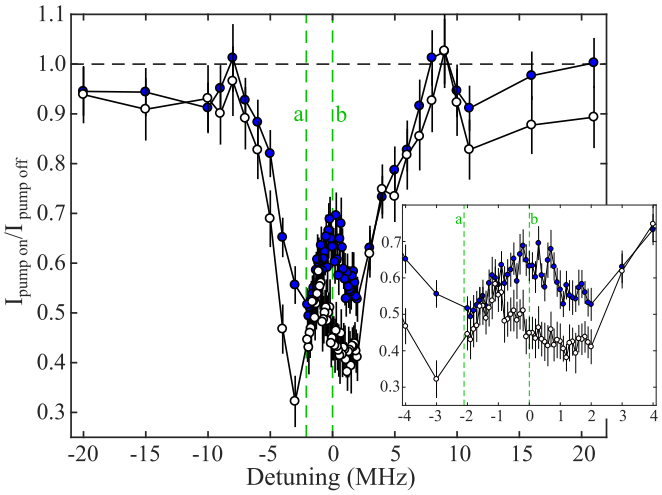

FIG. 8. The relative intensity change $I_{\mathrm{pump\,on}}/I_{\mathrm{pump\,off}}$ for SWAP (blue circles) and RAD deceleration (white circles) versus the pump-beam detuning. The parameters of the SWAP force are set to $f_{\mathrm{ramp}} = 500$ kHz, $\Delta_{\mathrm{ramp}} = 190\ \Gamma_{626}$, and $\Omega_0 = 29 \times 10^6\ \mathrm{s}^{-1}$, while the parameters of the RAD force are set to $\Omega_0 = 29 \times 10^6\ \mathrm{s}^{-1}$ and $\Delta_{\mathrm{RAD}} = -15.5\ \Gamma_{626}$ (green line labeled "a"). The green line labeled "b" indicates the resonance position of the $F = 10.5 \rightarrow F' = 10.5$ transition found by an independent spectroscopic measurement and it marks the pump-beam detuning used to obtain the data presented in Fig. 5(c). The pump-beam intensity is $I_{\mathrm{pump}} = 5.7\,\mathrm{I}_{\mathrm{sat}}$ and corresponds to a Rabi frequency of $2\pi \times 35$ kHz.

APPENDIX C: DEPENDENCE OF THE GROUND-STATE LOSSES ON THE PUMP-BEAM DETUNING

In Sec. II we show an increased robustness of the SWAP force against ground-state losses compared to the RAD force. For these measurements the frequency of the retroreflected pump beam is set to resonance with the $F = 10.5 \rightarrow F' = 10.5$ transition. For completeness, we study the pump-beam-detuning dependence of the ground-state losses. The relative intensity change $I_{\text{pump on}}/I_{\text{pump off}}$ after 3 ms SWAP and RAD slowing is measured for varying detunings and the results are presented in Fig. 8. Here $I_{\text{pump on}}$ ($I_{\text{pump off}}$) refers to losses being switched on (off). The experimental setup is identical to the one shown in Fig. 2(a). Overall the relative losses are larger for the RAD force than for the SWAP force, and for zero detuning the results are consistent with the data presented in Sec. II. Both spectra show a distinctive peak in the center of the broad loss dip. In the case of the SWAP force this peak is located roughly at zero detuning, which is the setting used for the data presented in Sec. II, while the peak in the RAD spectrum coincides with about half the RAD detuning which is 1.05 MHz. The nature of the observed feature and the structure of the observed spectra are significantly more complex than initially expected and will be the subject of future studies.

[1] H. Metcalf and P. Van der Straten, *Laser Cooling and Trapping* (Springer, New York, 1999).

[2] W. Ketterle, D. S. Durfee, and D. M. Stamper-Kurn, Making, probing and understanding Bose-Einstein condensates, *Proceedings of the International School of Physics "Enrico Fermi"*, Vol. 140 (IOS Press, 2018), pp. 67–176.

[3] W. Ketterle and M. W. Zwierlein, Making, probing and understanding ultracold Fermi gases, *Proceedings of the International School of Physics "Enrico Fermi"*, Vol. 164 (IOS Press, 2018), pp. 95–287.

[4] J. Eschner, G. Morigi, F. Schmidt-Kaler, and R. Blatt, Laser cooling of trapped ions, J. Opt. Soc. Am. B **20**, 1003 (2003).

[5] A. D. Ludlow, M. M. Boyd, J. Ye, E. Peik, and P. O. Schmidt, Optical atomic clocks, Rev. Mod. Phys. **87**, 637 (2015).

[6] H. Metcalf, Colloquium: Strong optical forces on atoms in multifrequency light, Rev. Mod. Phys. **89**, 041001 (2017).

[7] V. S. Voitsekhovich, M. V. Danileiko, A. Negriiko, V. Romanenko, and L. Yatsenko, Observation of a stimulated radiation pressure of amplitude-modulated light on atoms, JETP Lett. **49**, 161 (1989).

[8] J. Söding, R. Grimm, Y. B. Ovchinnikov, P. Bouyer, and C. Salomon, Short-Distance Atomic Beam Deceleration with a Stimulated Light Force, Phys. Rev. Lett. **78**, 1420 (1997).

[9] M. Partlow, X. Miao, J. Bochmann, M. Cashen, and H. Metcalf, Bichromatic Slowing and Collimation to Make an Intense Helium Beam, Phys. Rev. Lett. **93**, 213004 (2004).

[10] L. Yatsenko and H. Metcalf, Dressed-atom description of the bichromatic force, Phys. Rev. A **70**, 063402 (2004).

[11] C. Corder, B. Arnold, and H. Metcalf, Laser Cooling without Spontaneous Emission, Phys. Rev. Lett. **114**, 043002 (2015).

[12] T. Lu, X. Miao, and H. Metcalf, Bloch theorem on the Bloch sphere, Phys. Rev. A **71**, 061405(R) (2005).

[13] X. Miao, E. Wertz, M. G. Cohen, and H. Metcalf, Strong optical forces from adiabatic rapid passage, Phys. Rev. A **75**, 011402(R) (2007).

[14] D. Stack, J. Elgin, P. M. Anisimov, and H. Metcalf, Numerical studies of optical forces from adiabatic rapid passage, Phys. Rev. A **84**, 013420 (2011).

[15] M. A. Norcia, J. R. K. Cline, J. P. Bartolotta, M. J. Holland, and J. K. Thompson, Narrow-line laser cooling by adiabatic transfer, New J. Phys. **20**, 023021 (2018).

[16] J. A. Muniz, M. A. Norcia, J. R. K. Cline, and J. K. Thompson, A robust narrow-line magneto-optical trap using adiabatic transfer, arXiv:1806.00838.

[17] S. Snigirev, A. J. Park, A. Heinz, I. Bloch, and S. Blatt, Fast and dense magneto-optical traps for strontium, [Phys. Rev. A (to be published)], arXiv:1903.06435.

[18] G. P. Greve, B. Wu, and J. K. Thompson, Laser cooling with adiabatic transfer on a Raman transition, arXiv:1805.04452.

[19] W. C. Martin, R. Zalubas, and L. Hagan, Atomic energy levels—The rare-earth elements, NSRDS-NBS, Washington: National Bureau of Standards, U.S. Department of Commerce, 1978.

[20] W. Hogervorst, G. J. Zaal, J. Bouma, and J. Blok, Isotope shifts and hyperfine structure of natural dysprosium, Phys. Lett. A **65**, 220 (1978).

[21] M. Gustavsson, H. Lundberg, L. Nilsson, and S. Svanberg, Lifetime measurements for excited states of rare-earth atoms using pulse modulation of a cw dye-laser beam, J. Opt. Soc. Am. **69**, 984 (1979).

[22] A. L. Collopy, M. T. Hummon, M. Yeo, B. Yan, and J. Ye, Prospects for a narrow line MOT in YO, New J. Phys. **17**, 055008 (2015).

[23] A. Kramida, Yu. Ralchenko, J. Reader, and NIST ASD Team, NIST Atomic Spectra Database (ver. 5.5.6), available at https://physics.nist.gov/asd [2018, September 11] (National Institute of Standards and Technology, Gaithersburg, MD, 2018).

[24] S. H. Youn, M. Lu, U. Ray, and B. L. Lev, Dysprosium magneto-optical traps, Phys. Rev. A **82**, 043425 (2010).

[25] J. P. Bartolotta, M. A. Norcia, J. R. K. Cline, J. K. Thompson, and M. J. Holland, Laser cooling by sawtooth wave adiabatic passage, Phys. Rev. A **98**, 023404 (2018).

[26] F. Mühlbauer, N. Petersen, C. Baumgärtner, L. Maske, and P. Windpassinger, Systematic optimization of laser cooling of dysprosium, Appl. Phys. B **124**, 120 (2018).

[27] F. Gao, H. Liu, P. Xu, X. Tian, Y. Wang, J. Ren, H. Wu, and H. Chang, Precision measurement of transverse velocity distribution of a strontium atomic beam, AIP Adv. **4**, 027118 (2014).